Journal of Medicinal Chemistry

Article

pubs.acs.org/jmc

Ligand Efficiency Driven Design of New Inhibitors of *Mycobacterium tuberculosis* Transcriptional Repressor EthR Using Fragment Growing, Merging, and Linking Approaches

Baptiste Villemagne,[†,‡,§,∥,⊥] Marion Flipo,[†,‡,§,∥,⊥] Nicolas Blondiaux,[†,§,∥,⊥,#,∇,○] Céline Crauste,[†,‡,§,∥,⊥] Sandra Malaquin,[†,‡,§,∥,⊥] Florence Leroux,[†,‡,§,∥,⊥] Catherine Piveteau,[†,‡,§,∥,⊥] Vincent Villeret,[†,§,◆] Priscille Brodin,[†,§,∥,#,∇,○] Bruno O. Villoutreix,[▲,◇] Olivier Sperandio,[▲,◇] Sameh H. Soror,[+,△] Alexandre Wohlkönig,[+] René Wintjens,[□,◆] Benoit Deprez,*[,†,‡,§,∥,⊥] Alain R. Baulard,[†,§,∥,⊥,#,∇,○] and Nicolas Willand*[,†,‡,§,∥,⊥]

[†]Université Lille Nord de France, F-59044 Lille, France

[‡]Biostructures and Drug Discovery, INSERM U761, F-59006 Lille, France

[§]UDSL, F-59000 Lille, France

[∥]Institut Pasteur de Lille, F-59019 Lille, France

[⊥]PRIM, F-59006 Lille, France

[#]INSERM U1019, F-59019 Lille, France

[∇]CNRS UMR8204, F-59021 Lille, France

[○]Center for Infection and Immunity of Lille, F-59019 Lille, France

[◆]IRI, USR 3078 CNRS, F-59658 Villeneuve d'Ascq, France

[¶]Laboratory of Molecular Virology, IBBM, Université Libre de Bruxelles, 6041 Gosselies, Belgium

[+]Structural Biology Brussels and Molecular and Cellular Interactions, VIB, Brussels, Belgium

[□]Laboratoire de Chimie Générale, Institut de Pharmacie, Université Libre de Bruxelles, Brussels, Belgium

[▲]INSERM, UMRS 973, MTi, F- 75013 Paris, France

[◇]Univ Paris Diderot, F-75205 Paris, France

Supporting Information

ABSTRACT: Tuberculosis remains a major cause of mortality and morbidity, killing each year more than one million people. Although the combined use of first line antibiotics (isoniazid, rifampicin, pyrazinamide, and ethambutol) is efficient to treat most patients, the rapid emergence of multidrug resistant strains of *Mycobacterium tuberculosis* stresses the need for alternative therapies. Mycobacterial transcriptional repressor EthR is a key player in the control of second-line drugs bioactivation such as ethionamide and has been shown to impair the sensitivity of the human pathogen *Mycobacterium tuberculosis* to this antibiotic. As a way to identify new potent ligands of this protein, we have developed fragment-based approaches. In the current study, we combined surface plasmon resonance assay, X-ray crystallography, and ligand efficiency driven design for the rapid discovery and optimization of new chemotypes of EthR ligands starting from a fragment. The design, synthesis, and in vitro and ex vivo activities of these compounds will be discussed.

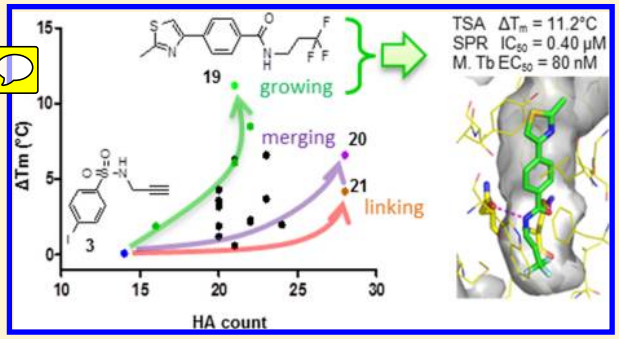

INTRODUCTION

Tuberculosis (TB) remains a major cause of mortality and morbidity, killing each year about 1.3 million people.[1] The pipeline of new antitubercular drugs developed to stop the progression of the epidemic has been enriched with new chemical entities in the last 10 years,[2−4] however, with the emergence of multidrug (MDR) and extensively drug-resistant (XDR) strains of *Mycobacterium tuberculosis*, there is an urgent need to complete this arsenal using alternative strategies. In antibacterial research and especially in tuberculosis, target-based high-throughput screening (HTS) approaches have not

Received: March 18, 2014
Published: May 12, 2014

   dx.doi.org/10.1021/jm500422b | J. Med. Chem. 2014, 57, 4876−4888

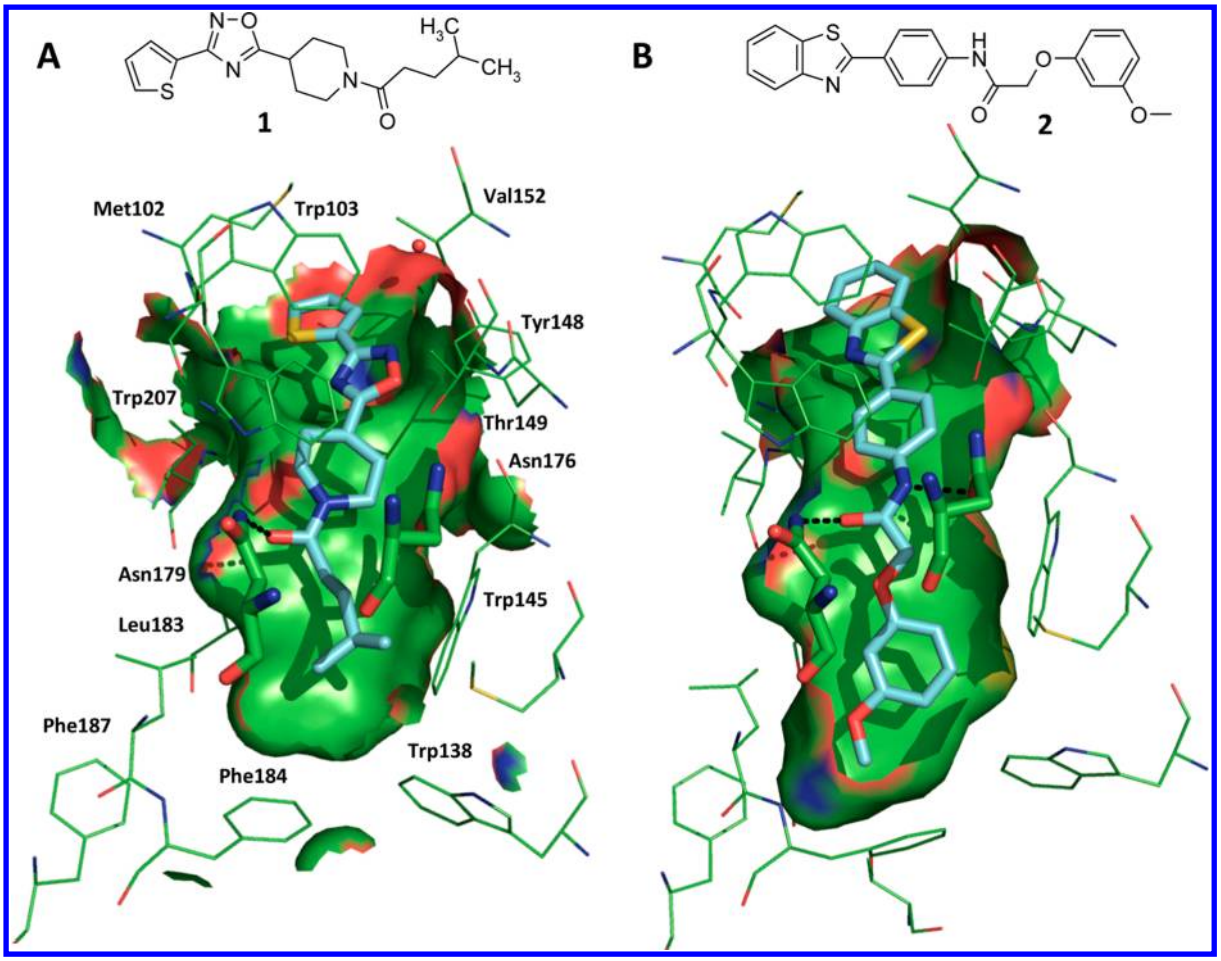

Figure 1. (A) X-ray structure representation of the ligand-binding pocket of EthR filled with compound **1** (PDB ID 3Q0V). (B) X-ray structure representation of the ligand-binding pocket of EthR filled with compound **2** (PDB ID 4DW6). Surface of ligand binding domain is highlighted. Hydrogen bonds with Asn179 and Asn176 are represented with dotted lines. Colors legend: blue (compound) or green (EthR) = carbon, dark blue = nitrogen, red = oxygen, yellow = sulfur. Images were generated with Pymol.

fully succeeded in delivering a substantial quantity of lead compounds to enrich the pipeline.[5,6] In parallel, fragment-based drug design (FBDD) has become an established approach in medicinal chemistry to discover hits and lead compounds in many areas[7,8] and particularly in infectious diseases, where conventional techniques may have failed. FBDD strategies were used for the discovery of inhibitors of *M. tuberculosis* proteins such as the tyrosine phosphatases PtpA[9,10] and PtpB,[11] pantothenate synthetase,[12] antigen 85C,[13] and CYP121.[14,15] However, none of these examples led to compounds showing whole cellular activities. More recently, Tran et al. discovered and optimized aromatic fragment-based inhibitors of type II dehydroquinase that inhibit the growth of *M. tuberculosis* in the low-micromolar range.[16] Finally, Surade et al. used a structure-guided fragment linking strategy to discover an EthR ligand able to boost ethionamide activity when tested at 1 μM.[17]

One of the major advantages to use fragments as starting molecules relies on their small size (usually less than 17 non-hydrogen atoms) and low molecular weight (MW < 300 g·mol^{-1}). They exhibit therefore better physicochemical properties, especially solubility, than lead-like or drug-like compounds. Because *M. tuberculosis* is an intracellular pathogen, these properties make fragments ideal tools to favor their penetration into the phagosomes of macrophages that harbor the bacteria and eventually through the waxy and thick *M. tuberculosis* cell wall itself.[18] This fundamental advantage compensates for low affinity and activity of initial hit fragments which can be optimized in a second round of synthesis, keeping molecular weight and size as low as possible while improving ligand efficiency.

In the present study, we searched for new potent chemical series of EthR ligands and ethionamide boosters using fragment-based approaches. Ethionamide is a second-line drug used to treat MDR-TB that is resistant to both first-line drugs isoniazid and rifampicin. It is a prodrug bioactivated by the *M. tuberculosis* flavin-containing monooxygenase EthA that triggers the formation of an ethionamide−NAD adduct.[19] This active ethionamide−NAD adduct inhibits InhA and thus the synthesis of mycolic acids. EthR, a transcriptional repressor of the TetR family that inhibits the expression of EthA, was identified as the major factor of the mycobacterial molecular mechanism contributing to intrinsic ethionamide low activity.[20,21] Recently, we demonstrated that EthR is a valuable target to boost ethionamide bioactivation. We identified potent drug-like EthR ligands that boost in vitro and in vivo ethionamide activity using structure-based design[22−24] and high-throughput screening.[25] We ended up with two distinct families of ligands, one bearing an acylated 1,2,4-oxadiazolylpiperidinyl scaffold and the second one presenting a *N*-phenylphenoxyacetamide motif. Representative members of

dx.doi.org/10.1021/jm500422b | *J. Med. Chem.* 2014, 57, 4876−4888

the two series, compounds **1** (BDM31369)[23] and **2** (BDM31827),[25] were successfully cocrystallized with EthR at a resolution of 2.0 Å. The two ligands occupy the same region of the ligand binding domain and are both H-bonded to Asn179. Compound **2** also binds to the side chain of Asn176 (Figure 1). This structural information was used to further explore the ligand binding domain of EthR. Starting from a small EthR ligand and using a combination of X-ray crystallography, in silico screening, as well as fragment-growing, merging, and linking approaches, we discovered a new chemical family of potent EthR ligands. We succeeded in improving by 400-fold activity of our initial fragment thanks to key modifications. This work led to the rapid discovery of compound **19** (BDM43266), which displays high efficacy through a new binding mode.

RESULTS AND DISCUSSION

4-Iodo-*N*-prop-2-ynylbenzenesulfonamide (compound **3**) is a small molecule that was discovered while probing the flexibility of the long and linear ligand binding domain of EthR using in situ click-chemistry.[26] The compound **3** can be considered as a fragment as it follows the "rule of 3" (Table 1),[27,28] with less than 3 H-bond acceptor and H-bond donor atoms, a calculated logP less than 3, 14 heavy atoms, and a low molecular weight (<300 g·mol^{-1}) without taking the mass of iodine atom into account. Interestingly, it also displayed a very high solubility (>200 μM).

Table 1. Physicochemical Properties of Compound 3

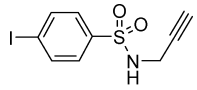

Compound 3

MW (g·mol^{-1})	194.2 (+ 126.9 for iodine)
H-Acc	2
H-Don	1
cLogP	2.26
Nrot	3
PSA (A^2)	54.55
non-hydrogen atoms	14
solubility (μM)	>200

Moreover, the compound **3** was confirmed as a weak binder of EthR. Using the thermal shift assay developed earlier to evaluate the affinity of ligands to EthR, we measured a shift of temperature between holo and apo-EthR, expressed as ΔT_m, of 0.1 °C.[26] Its capacity to inhibit EthR−DNA interaction, measured by surface plasmon resonance assay (SPR),[24] was not negligible as it showed an IC_{50} equal to 160 μM. More importantly, the binding mode of the compound **3** to EthR was revealed by cocrystallization with the protein. The structure of the complex was determined at a resolution of 2.0 Å. X-ray analysis of the crystal structure revealed the presence of two copies of the compound **3** embedded in each binding pocket of the homodimeric structure of EthR (Figure 2).

The binding domain filled by the two molecular entities adopts a "Y-like" shape with three distinct subdomains called D1, D2, and D2′. D1 represents the "known binding domain", where all described EthR ligands have been shown to fit.[22−24] This hydrophobic pocket is lined with backbones of Phe110, Phe114, Met142, Ile107, and Trp207, and displays at the bottom a gate formed by the side chains of Trp138 and Phe184. These two residues have been shown to delimit a secondary pocket of the protein accessible to longer ligands.[17,25,26] In this D1 domain, the compound **3** is sandwiched between Trp207 and Phe110, while its sulfonamide group is H-bonded to Asn179. The newly occupied subpocket D2 is defined by backbones of Met102, Trp103, Val152, and Tyr148 that is H-bonded to the sulfonamide moiety of the second molecule of the compound **3**. The sulfonamide nitrogen of the fragment also participates in water-mediated interactions with Leu90 and Asn93. Finally, a third subpocket D2′ composed by Pro94, Thr105, Ala95, and Leu90 is invaded by the acetylenic tail. The original binding of the compound **3** in two distinct pockets of the ligand binding domain of EthR was

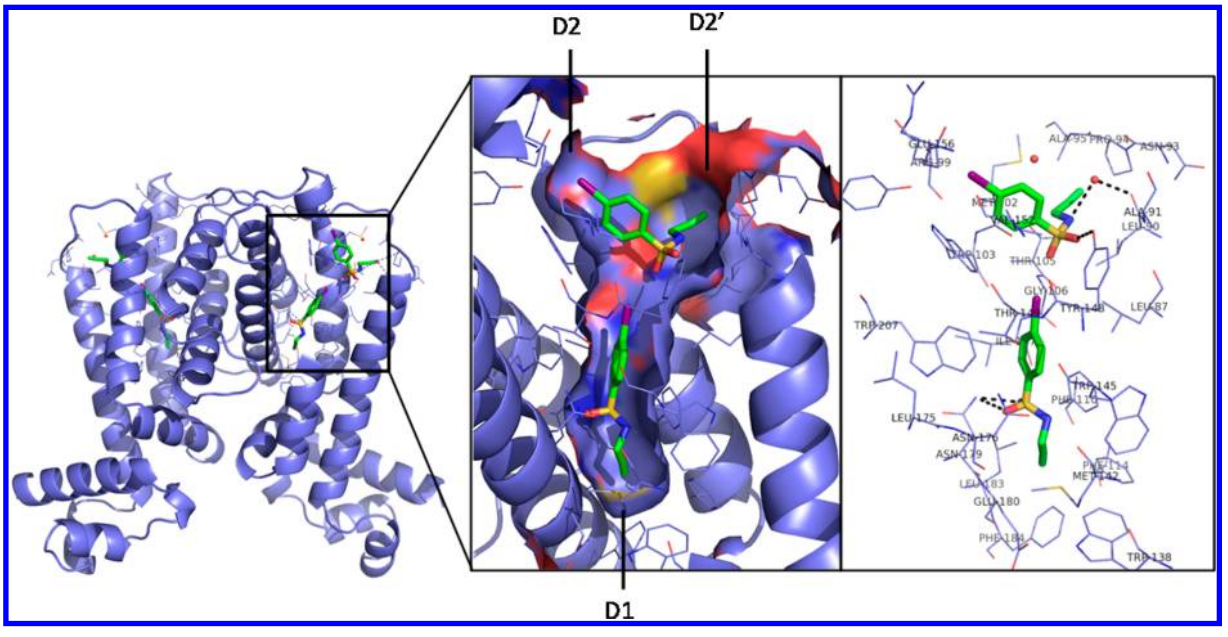

Figure 2. Simplified view of the compound **3** cocrystallized in two distinct regions of the ligand binding domain of EthR. Black dashed lines indicate the hydrogen bond interactions of the ligand with the backbone residues and with water molecules. Images were generated with Pymol.

dx.doi.org/10.1021/jm500422b | J. Med. Chem. 2014, 57, 4876−4888

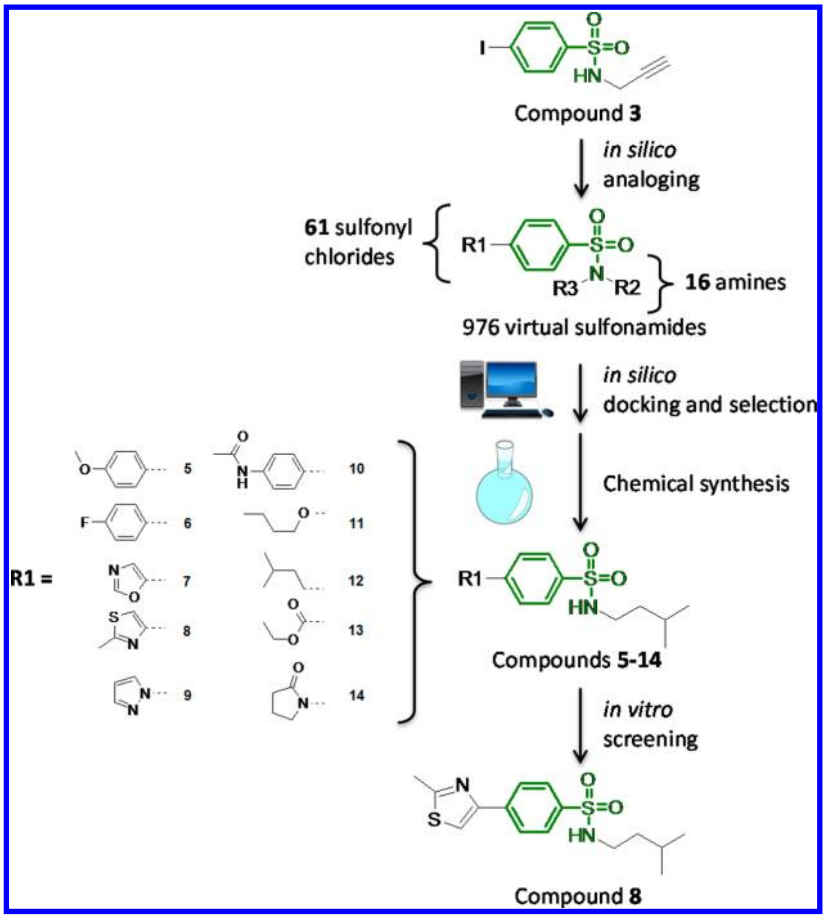

Figure 3. Fragment-growing strategy: from virtual design and selection to in vitro validation.

a nice opportunity to optimize this small fragment, either by starting a growing strategy or by linking two scaffolds together. The fragment-growing strategy was focused on pocket D1 and initiated with a fragment evolution using the synthesis of a virtual library based on the arylsufonamide scaffold to allow the introduction of a broad diversification of the starting molecule. On the basis of structural data, rational chemical modifications were performed and compounds were validated throughout the optimization process as EthR ligands using SPR. Impacts of modifications on binding mode were confirmed by X-ray diffraction of crystals of holo-protein complexes. In parallel, fragment merging and linking strategies were performed to design compounds that not only bind to subpocket D1 but also interact with new defined subpockets D2 and D2′.

Fragment Growing Strategy. Following the identification of the compound **3**, we performed its chemical optimization using a fragment growing approach with the aim of improving ligand efficiency. As we knew from past studies that anchoring via H-bond to Asn179 and occupancy of the ligand binding domain near Gly106 is crucial for EthR inhibition, we focused our growing-based optimization on the design of molecules that could target the D1 pocket. To guide the design of potent analogues, we built a virtual library of 976 members based on arylsulfonamide framework, the key molecular feature that allows compound **3** to interact in the D1 pocket. As this ligand binding domain is thin and linear, the chemical diversity was introduced in two opposite directions. We virtually modified the nature of the sulfonamide chain by introducing small hydrophobic substituents, and we allowed larger modifications at the para position of the phenyl ring. The library was synthesized in silico by coupling 16 small amines (MW > 100 g·mol^{-1}) with 61 commercially available 4-substituted arylsulfonyl chlorides using the Accelrys software Pipeline Pilot (Figure 3).

We then developed an in silico docking procedure that took into account the previously acquired knowledge on interactions between EthR and its ligands. The occupancy of pockets D2 and D2′ by the compound **3** (EthR-**3**) was a yet undescribed structural feature, whereas the occupation of D1 has been described for high affinity ligands cocrystallized previously. This was for example the case for compound **1** (EthR-**1**, PDB code 3Q0V, Figure 1A), which showed a favorable occupancy of the D1 pocket. To take advantage of these two structures, which collectively allowed an optimized occupancy of the EthR binding pocket for the newly designed compounds of our virtual library, we performed docking on each cocrystal structures of EthR and combined the results. Using the software Surflex 2.415, we docked the 976 members of the virtual library on the two unoccupied conformations of EthR, and we eventually filtered out compounds having a score below a predicted pK_i of 8. We obtained 142 ligands coming from the docking on EthR-**1** and 148 ligands issued from the docking on EthR-**3**. We selected from the two lists the 75 ligands that were able to accommodate both conformations of the protein, and we finally inspected manually the docking poses of each fragment to select among the 75 ligands those having favorable protein−ligand contacts such as hydrogen bonds (mainly with the side chain of Asn179) and hydrophobic contacts. Among

dx.doi.org/10.1021/jm500422b | J. Med. Chem. 2014, 57, 4876−4888

the 75 compounds, 10 (1% of the whole library) resulted from sulfonylation of isopentylamine (Figure 3). The docking simulations proposed that the substituted aliphatic chain would fit perfectly at the bottom of D1, which is in agreement with our previous work.[23]

These 10 compounds (**5**–**14**) were selected and synthesized, according to Scheme 1, from the reaction of 10 different

Scheme 1. Synthesis of Sulfonamide and Amide Compounds for Structure–Activity Relationships (SAR) Studies[a]

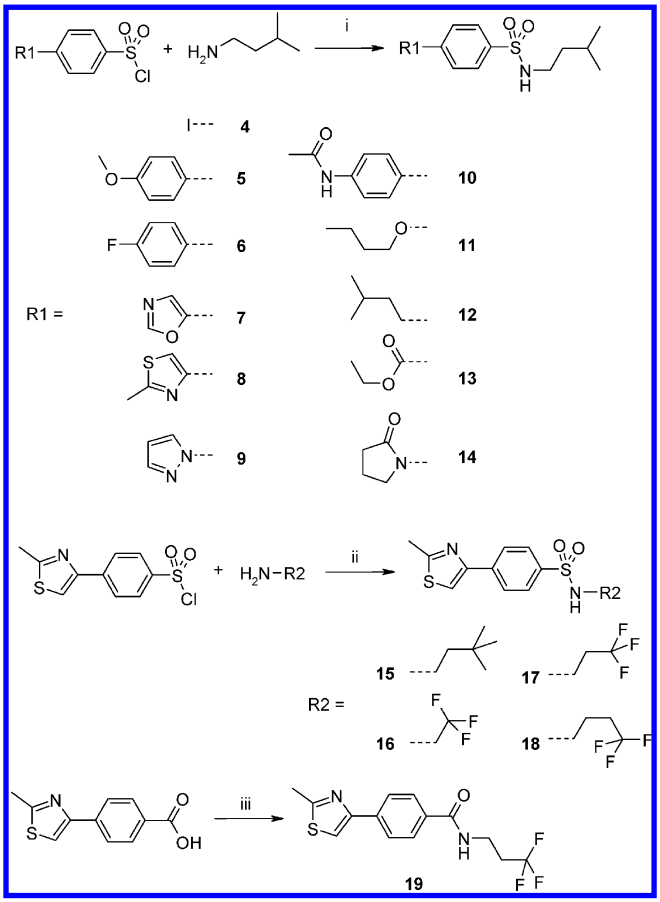

[a]Reagents and reaction conditions: (i) 3-methylbutan-1-amine (1.0 equiv), sulfonyl chloride (1 equiv), 4-methylmorpholine (3 equiv), anhydrous DMF, RT, 2 h; (ii) 4-(2-methylthiazol-4-yl)benzene-1-sulfonyl chloride (1 equiv), amine (1–1.5 equiv), 4-methylmorpholine (NMP, 5 equiv), anhydrous DMF, RT, 2 h; (iii) 3,3,3-trifluoropropylamine hydrochloride (1.1 equiv), *O*-benzotriazole-*N*,*N*,*N*′,*N*′-tetramethyl-uronium-hexafluoro-phosphate (HBTU, 1.2 equiv), *N*-hydroxybenzotriazole (HOBt, 1.5 equiv), *N*,*N*-diisopropylethylamine (DIEA, 3 equiv), DMF, RT, 2 h.

arylsulfonyl chlorides with 3-methylbutan-1-amine in the presence of 4-methylmorpholine at room temperature in anhydrous *N*,*N*-dimethylformamide (DMF). 4-Iodo-*N*-isopentylbenzenesulfonamide (compound **4**), the direct analogue of compound **3**, with an isopentyl tail, was synthesized to evaluate the impact of this substitution on in vitro activity. Compounds **3**–**14** were screened against EthR using the thermal shift assay (Table 2). In agreement with in silico docking, the replacement of the propargyl chain (compound **3**) by isopentyl (compound **4**) increased melting temperature by 1.8 °C. The replacement of iodine by oxazole, pyrazole, or pyrrolidinone (compounds **7**, **9**, and **14**) did not increase affinity to the target. On the

Table 2. Activities of Compounds 3–14

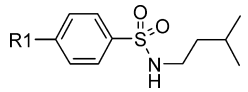

Compound Id	R1	Score	ΔTm (°C)[a]	EC_{50} (μM)[b]	HA[c]
3	-	5.4	0.1	>10	14
4	I---	7.7	1.9	>10	16
5		9.3	3.7	>10	23
6		9.4	2.2	>10	22
7		8.7	1.2	>10	20
8		9.3	6.1	5.7	21
9		8.6	1.9	>10	20
10	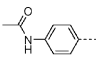	8.5	2.0	>10	24
11		9.3	3.6	>10	20
12		10.0	3.2	6.3	20
13		8.1	4.3	10	20
14		8.9	0.6	>10	21

[a]ΔT_m data were obtained using thermal shift assay. [b]EC_{50} represents the concentration of ligand that allows ethionamide at 0.1 μg/mL (normal MIC/10) to inhibit 50% of *M. tuberculosis* growth in macrophages. [c]HA = number of non-hydrogen atoms.

contrary, the replacement of iodine (compound **4**) by 2-methylthiazol-4-yl (compound **8**) shifted melting temperature by 4.2 °C. Lower increases were observed with the introduction of hydrophobic aliphatic chain (compound **12**) or hydrophilic alkyl ester and ether chains (compounds **13** and **11**). Addition of a bulkier aromatic ring (compounds **5**, **6**, and **10**) was less tolerated. To evaluate the ability of these compounds to cross biological membranes and to reach their target in a cellular assay, the 10 EthR ligands were tested in vitro on *M. tuberculosis* infected macrophages. The assay was performed in the presence of subactive concentrations of ethionamide (0.1 μg/mL of ethionamide = MIC/10), which allows determination of a compound's efficacy to boost antibiotic activity (expressed as EC_{50}).[23] Moreover, we used this assay to confirm that the compounds alone were inactive and not toxic for macrophages. Ligand efficiency index (LE) was used to compare compounds and expressed using the following equation LE = $((1.37 \times pEC_{50})/(HA)$ where HA is the number of heavy atoms.[29,30]

At this stage, three compounds (**8**, **12**, and **13**) had EC_{50} ranging between 5 and 10 μM. Compound **8**, the most active analogue in both assays (ΔT_m = 6.1 °C, EC_{50} = 5.7 μM), was successfully cocrystallized with EthR, and the structure was

dx.doi.org/10.1021/jm500422b | J. Med. Chem. 2014, 57, 4876–4888

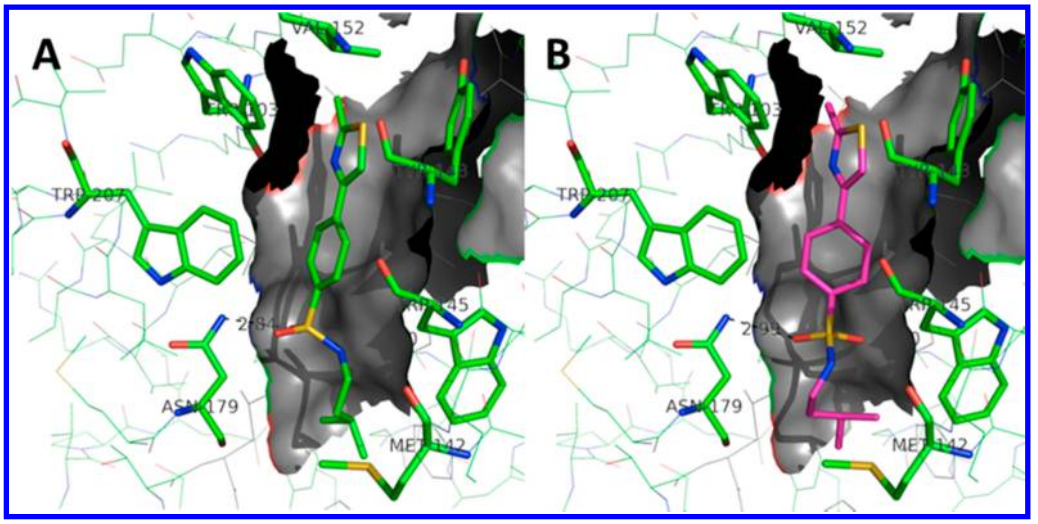

Figure 4. (A) X-ray structure of compound **8** (green) cocrystallized with EthR (B). Docked pose of compound **8** (magenta) with X-ray structure of EthR. The root-mean-square deviation (RMSD) between the docked pose and the experimental bioactive conformation of the compound **8** is equal to 1.15 Å. (PDB ID 4M3F) Pivotal hydrogen bonds between the compound **8** and Asn179 are respectively 2.84 and 2.99 Å.

Table 3. Activities of Compounds 15−19

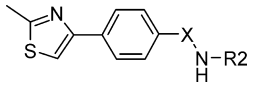

Compound Id	X	R2	ΔTm (°C)[a]	IC_{50} (μM)[b]	EC_{50} (μM)[c]	HA[d]	LE[e]	Solubility (μg/mL)[f]
8 (ref)	SO_2		6.1	4.9	5.7	21	0.34	6.6
15	SO_2		2.3	-	>20	22	-	-
16	SO_2		6.3	-	7.9	21	0.34	-
17	SO_2		8.5	0.55	0.29	22	0.41	14.5
18	SO_2		6.6	-	>2.5	23	-	-
19	CO		11.2	0.40	0.08	21	0.47	14.7

[a]ΔT_m were obtained using thermal shift assay. [b]IC_{50} were determined by SPR and represents the concentration of ligand that inhibits 50% of the interaction of EthR with its promoter [c]EC_{50} represents the concentration of ligand that allows ethionamide at 0.1 μg/mL (normal MIC/10) to inhibit 50% of *M. tuberculosis* growth in macrophages. [d]HA = number of non-hydrogen atoms. [e]LE = $-1.37\log(EC_{50})$/HA. [f]Solubilities were determined at pH 7.4.

determined at a resolution of 2.0 Å (Figure 4A). X-ray diffraction data revealed that as predicted by docking (Figure 4B), the sulfonamide group was H-bonded to the side chain of Asn179. The phenyl scaffold was facing Trp207 and Phe110, while the thiazole ring was surrounded by Trp103, Tyr148, Val152, and Leu87. The methyl substituent was pointing to Met102, which had flipped to occupy the subpocket D2′. We also observed that the ligand fitted well the bottom of the ligand binding domain as expected.

To improve ligand efficiency, we explored chemical modifications specifically designed to impact weakly on the molecular weight. We kept the 2-methylthiazol-4-yl moiety, and we first replaced the isopentyl chain of the compound **8** by a more substituted 3,3-dimethylbutyl chain or by trifluoroalkylated linear chains (compounds **15**−**18**, Table 3). Increase of steric hindrance in the bottom of the D1 pocket by the introduction of a *tert*-butyl group led to a loss of activity (compound **15**, ΔT_m = 2.3 °C and EC_{50} > 20 μM). Substitution of the isopentyl chain by a trifluoropropyl chain leading to compound **17** increased significantly the affinity (ΔT_m = 8.5 °C) and by 20-fold the efficacy (EC_{50} = 0.29 μM, LE = 0.41). Moreover, the fluorinated compound **17** also exhibited an improved solubility (14.5 μg/mL) compared to compound **8** (6.6 μg/mL), in agreement to what was already observed with previous identified EthR ligands or in the literature.[23,24,31] Shorter (compound **16**) or longer (compound **18**) trifluoromethylated analogues were less active (EC_{50} > 2.5 μM). Compound **17** was 9 times more potent than the

dx.doi.org/10.1021/jm500422b | J. Med. Chem. 2014, 57, 4876−4888

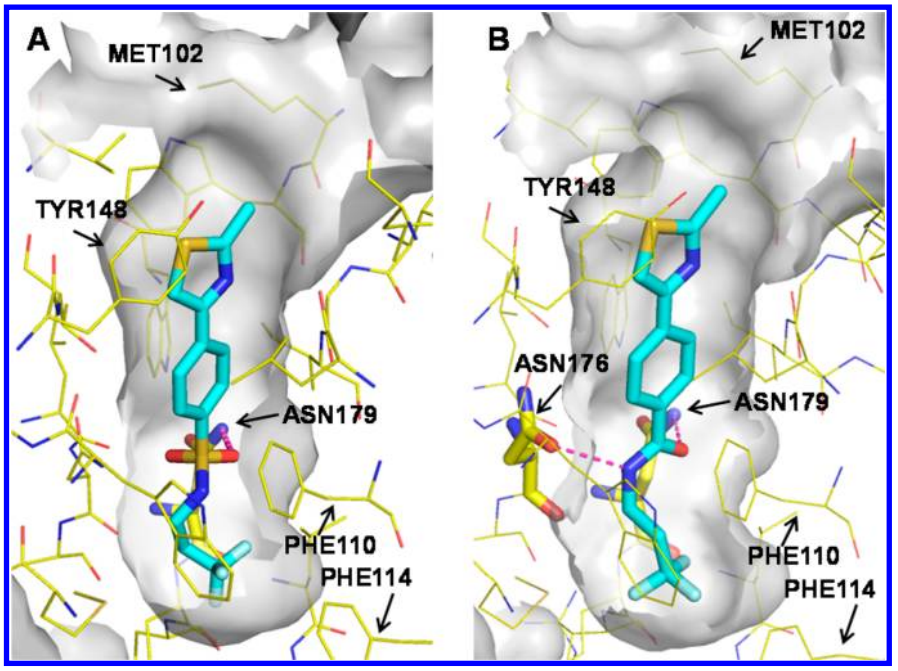

Figure 5. X-ray structures representation of the ligand-binding pocket of the repressor EthR occupied by compounds **17** (A) (PDB ID 4M3G) and **19** (B) (PDB ID 4M3B). The surface of the ligand binding domain is highlighted and hydrogen bond with residue side chains are represented with pink dashed lines. Colors legend: blue (compound) or yellow (EthR) = carbon, dark blue = nitrogen, red = oxygen, yellow = sulfur, white = fluor. Images were generated with Pymol.

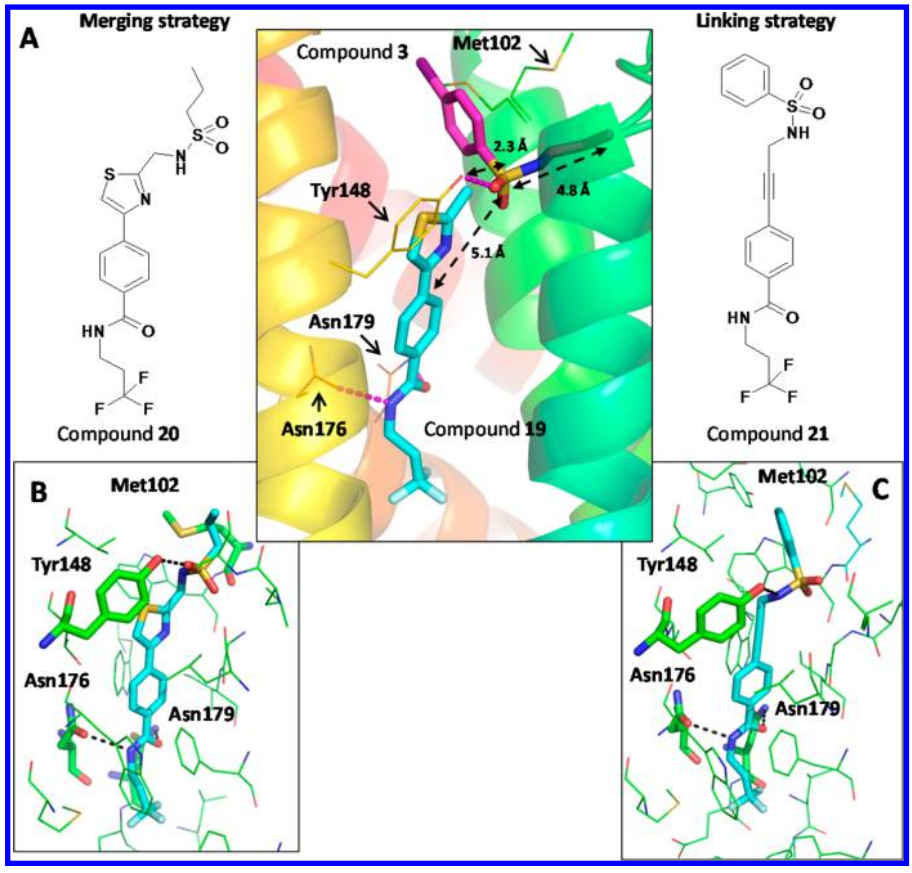

Figure 6. (A) Structures of the two compounds (**20** and **21**) designed by superimposition of X-ray structures of the compound **19** and the upper copy of the compound **3** in complex with EthR. Key residues interacting with the two ligands are labeled. (B) X-ray structure of the compound **20** (PDB ID 4M3E). (C) X-ray structure of the compound **21** (PDB ID 4M3D).

compound **8** in SPR assay (IC_{50} = 0.55 vs 4.9 μM). The X-ray crystal structure of the complex of **17** with EthR was determined at a resolution of 2.20 Å. While the aromatic moiety of the molecule conserves the same binding mode as

dx.doi.org/10.1021/jm500422b | J. Med. Chem. 2014, 57, 4876−4888

Scheme 2. Synthesis of Merging and Linking Compounds 20 and 21[a]

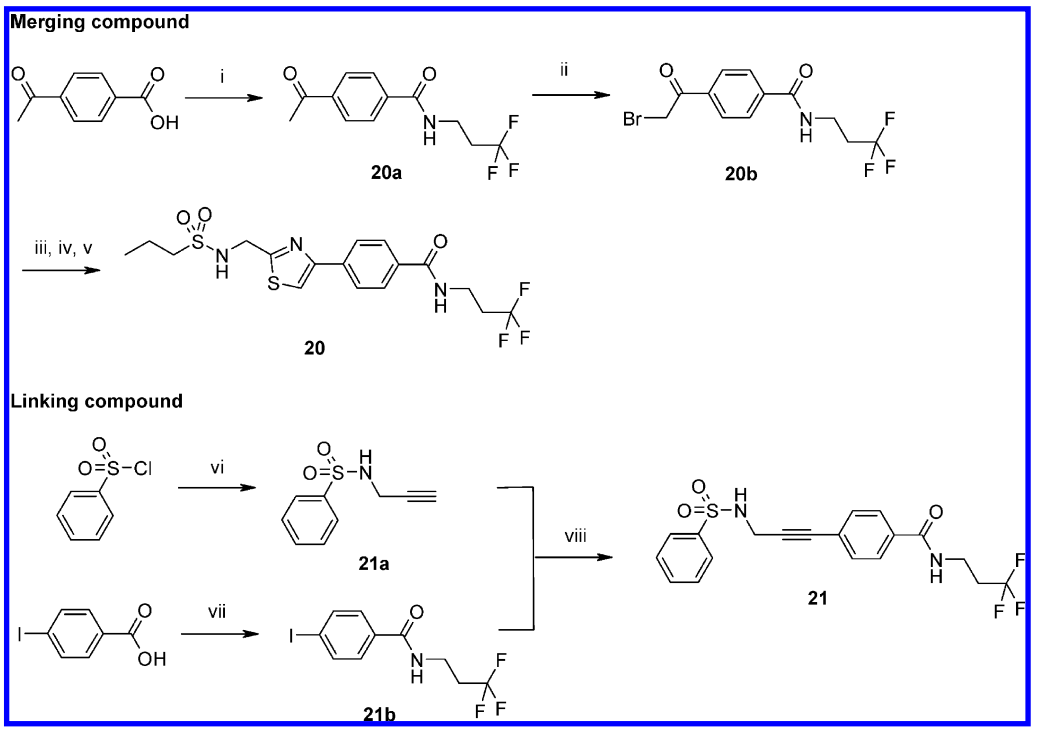

[a]Reagents and reaction conditions: (i) 3,3,3-trifluoropropylamine hydrochloride (1 equiv), HBTU (1.2 equiv), HOBt (0.1 equiv), DIEA (4 equiv), DMF, RT, 2 h; (ii) trimethylphenylammonium tribromide (1 equiv), DCE/MeOH (5/2), 50 °C, 3 h; (iii) *N*-benzyloxycarbonylglycine thioamide (1 equiv), THF, 70 °C, 3 h; (iv) 25% HBr in acetic acid, RT, 1 h; (v) propane1-sulfonyl chloride (1.5 equiv), NMP (4 equiv), DCM, RT, 1 h; (vi) propargylamine (1.2 equiv), DIEA (4 equiv), DCM, RT, 2 h; (vii) 3,3,3-trifluoropropylamine hydrochloride (1 equiv), HBTU (1.2 equiv), HOBt (0.2 equiv), DIEA (4 equiv), DMF, RT, 2 h; (viii) bis(triphenylphosphine)palladium(II) dichloride ($PdCl_2(PPh_3)_2$, 0.05 equiv), copper iodide (CuI, 0.9 equiv), triethylamine (2.9 equiv), DMF, 80 °C, overnight.

compound **8**, the terminal trifluoropropyl chain has slightly moved to point toward Phe114 at the bottom of the D1 subpocket (Figure 5A).

To further optimize the potency of our compounds, we replaced the sulfonamide function by an amide linker. The compound **19** (Table 3) showed gains in all activities (ΔT_m = 11.2 °C and EC_{50} = 80 nM, LE = 0.47) while keeping equal solubility (14.7 μg/mL). The IC_{50} value of the compound **19** was also slightly improved (IC_{50} = 0.40 μM) compared to **17** (IC_{50} = 0.55 μM). This increase of activity may be due to the formation of a new H-bond between the hydrogen atom of the amide linker and the oxygen atom of Asn176 side chain as revealed by the X-ray crystal structure of the complex, determined at a resolution of 2.00 Å (Figure 5B). Importantly, this result shows for the second time that an EthR ligand can be stabilized in the EthR pocket by H-bonding to asparagines Asn179 and Asn176 at the same time.[25]

Combining in silico and X-ray structure guided optimization approaches, we rapidly improved the potency of our initial fragment and identified a very efficient lead compound that increases by 10-fold the activity of ethionamide in *M. tuberculosis* infected macrophages at a concentration of 80 nM.

Fragment-Merging and Linking Strategies. In a further attempt to probe the ligand binding domain of EthR in D2 and D2′ subpockets, we superimposed the X-ray structure of the compound **19** with the one of compound **3** binding to D2 and D2′ (Figure 6A). As the methyl group of the compound **19** was found to be 2.3 Å distant from the sulfur atom of the fragment, we therefore designed the propylsulfonamide analogue **20** as a merged compound which was supposed to be more flexible and accommodate the D2 subpocket while keeping the H-bond interaction with Tyr148 and at the same time maintaining initial interactions in the D1 pocket with Asn179. Interestingly, we also noticed that the distance between the sulfur atom and the terminal carbon atom of the alkyne chain was almost equal to the distance between the sulfur atom and the C5 carbon of the thiazole ring (as shown in Figure 6). We thus thought that a propargylamine linker could be suitable to connect the phenylsulfonyl function to the para position of 3,3,3-trifluoropropylbenzamide scaffold without losing its initial binding mode. This led to the linked compound **21**. The two merging/linking compounds were synthesized according to Scheme 2.

Compounds **20** and **21** were evaluated in our different assays (Table 4) and cocrystallized with the protein (respective resolutions were 2.11 and 1.90 Å). As expected, the H-bond between the sulfonamide moiety and the hydroxyl group of Tyr148 was observed for the two analogues (Figure 6B,C). However, they bound in a different manner. Indeed, compound **20** bound one oxygen atom of its sulfonamide group to the Tyr148 as the compound **3** did, while the NH group of the compound **21** is now H-bonded to Tyr148. Moreover, we observed a new interaction between the compound **20** and Met102, which slightly moved its side chain to present its sulfur atom to interact with the NH group of the sulfonamide moiety. In the bottom of the pocket, the amide group of the two compounds was also H-bonded to both Asn176 and 179.

Finally, the two compounds **20** and **21** exhibited improved activities compared to initial fragments. However, these compounds were found to be poorly soluble and less efficient

dx.doi.org/10.1021/jm500422b | *J. Med. Chem.* 2014, 57, 4876−4888

Table 4. Activities of Compounds 20 and 21

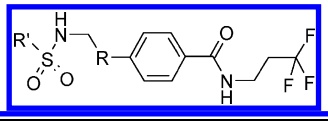

Cpd	R'	R	ΔTm (°C) [a]	IC_{50} (μM) [b]	EC_{50} (μM) [c]	HA [d]	LE [e]	Solubility (μg/mL) [f]
20			6.6	0.56	0.32	28	0.23	1.3
21			4.2	3.9	0.23	28	0.24	3.0

[a] ΔT_m were obtained using thermal shift assay. [b] IC_{50} were determined by SPR and represents the concentration of ligand that inhibits 50% of the interaction of EthR with its promoter. [c] EC_{50} represents the concentration of ligand that allows ethionamide at 0.1 μg/mL (normal MIC/10) to inhibit 50% of *M. tuberculosis* growth in macrophages. [d] HA = number of non-hydrogen atoms. [e] LE = $-1.37\log(EC_{50})/HA$. [f] Solubility was determined at pH 7.4.

than compound **19**, optimized through the growing strategy. This lack of solubility is probably due to the increase of the number of hydrophobic atoms, which is unavoidable using merging and linking strategies with a ligand binding domain rich in lipophilic residues.

Even if we succeeded in optimizing potencies of the compounds compared to the initial fragments using the linking and merging strategies, these two strategies failed in affording compounds with high ligand efficiency index. In these strategies, we were facing two problems: a decrease of solubility while increasing number of atoms and functional groups and a limitation in the choice of linkers to connect the two scaffolds while maintaining key interactions. Therefore, in the present case, the growing strategy was shown to provide more diversity than linking and merging strategies to explore the rigid ligand binding domain of this transcriptional regulator.

CONCLUSION

Through three fragment-based approaches, we optimized a fragment into potent ligands of the mycobacterial transcriptional regulator EthR. This process led to the conversion of a micromolar affinity fragment into low nanomolar affinity ligands of EthR and low nanomolar boosters of ethionamide activity. By combining crystallography studies of the protein−ligand complexes, in silico design to explore the chemical diversity of compounds, and eventually determination of ligand potency by in vitro and cellular assays, we could follow a rational path of optimization which led to the discovery of optimal EthR ligands. Of the three approaches, the "growing" strategy was particularly successful, leading to a new chemical class of EthR ligands, with compound **19** showing optimized activity (ΔT_m = 11.2 °C, IC_{50} = 0.40 μM and EC_{50} = 0.08 μM), high ligand efficiency (LE = 0.47), and good solubility. Optimization of the pharmacokinetic properties of the lead to perform in vivo experiments will be reported in due course.

EXPERIMENTAL SECTION

Biology. *Thermal Shift Assay (TSA).* The fluorescent dye SYPRO Orange (Invitrogen) was used to monitor protein unfolding. The thermal shift assay was conducted in a Lightcycler 480 (Roche). The system contained a heating/cooling device for temperature control and a charge-coupled device (CCD) detector for real-time imaging of the fluorescence changes in the wells of the microplate. The final sample concentrations were 10 μM EthR, 2.5× SYPRO Orange, 1% DMSO, and 20 μM ligand in the EthR buffer (10 mM Tris/HCl, 300 mM NaCl, pH 7.5, 0.1 mM EDTA). The samples were heated from 37 to 85 °C with a heating rate of 0.04 °C/s. The fluorescence intensity was measured at Ex/Em: 465/510 nm. The data were obtained using the algorithmic program Wavemetrics Igor by applying the following designed procedure: the fluorescence intensity of each well/sample is plotted as a function of the temperature. Then, the 1D-numerical derivative of these curves is calculated. At last, the maximum data values, corresponding to the inflection points (T_m), is extracted to give T_m in a table and in a graph.

IC_{50} Determination Using Surface Plasmon Resonance (SPR). Interactions between EthR and the *ethA* promoter region were analyzed using "Research Grades Streptavidin-Coated Sensor Chips (Sensor Chip SA, Biacore Inc.)" on a Biacore 3000 instrument (Biacore, Uppsala, Sweden). The 106-bp biotinylated DNA fragment overlapping the *ethA*/*ethR* intergenic region was obtained by polymerase chain reaction (PCR), purified by agarose gel electrophoresis, and immobilized onto the SA sensor chip. The biotinylated DNA fragment was injected in one channel of the chip at 150 ng/mL to obtain a 75 resonance unit (RU) stable fixation to immobilized streptavidin. Another channel of the chip was loaded with a biotinylated double-stranded 113-bp long irrelevant DNA fragment (+14 to +127 fragment of the *Escherichia coli* bla gene PCR amplified using oligonucleotides O-343, TTTCCGTGTCGCCCTTATTCC, and O-344, CCACTCGTGCACCCAACTGAT, and pUC18 as substrate). Binding of EthR to the immobilized DNA was performed at 25 °C in 10 mM Tris-HCl (pH 7.5), 200 mM NaCl, 0.1 mM EDTA, 1 mM DTT, and 1% DMSO at a flow rate of 20 μL/min for 3 min. Specific interaction (Supporting Information) between EthR and the 106-bp DNA fragment was defined as the signal difference between both channels. For dose−response curves establishment, the test compounds were serially diluted in the binding buffer containing 590 nM EthR, incubated 5 min at 37 °C, then injected in the Biacore at a flow rate of 20 μL/min for 3 min. Supporting Information values were measured at the end of the injection period and used to calculate the inhibition of protein−DNA interaction. IC_{50} values were determined using GraphPad Prism software.

Intracellular Assay. Raw264.7 macrophages (10^8 cells) were infected with H37Rv-GFP suspension at a multiplicity of infection (MOI) of 1:1 in 300 mL for 2 h at 37 °C with shaking (100 rpm). After two washes by centrifugation at 1100 rpm for 5 min, the remaining extracellular bacilli from the infected cells suspension were killed by a 1 h amikacin (20 μM, Sigma, A2324-5G) treatment. After a final centrifugation step, 40 μL of *M. tuberculosis* H37Rv-GFP colonized macrophages were dispensed with the Wellmate (Matrix) into 384-well Evotec plates preplated with 10 μL of compound mixture diluted in cell medium and incubated for 5 days at 37 °C, 5% CO_2. Macrophages were then stained with SYTO 60 (Invitrogen, S11342) for 1 h followed by plate sealing. Confocal images were recorded on an automated fluorescent ultrahigh-throughput microscope Opera (Evotec). This microscope is based on an inverted microscope architecture that allows imaging of cells cultivated in 96- or 384-well microplates (Evotec). Images were acquired with a 20× water immersion objective (NA 0.70). A double laser excitation (488 and 635 nm) and dedicated dichroic mirrors were used to record green fluorescence of mycobacteria and red fluorescence of the macrophages on two different cameras, respectively. A series of four pictures at the center of each well were taken, and each image was then processed using dedicated image analysis.[32−34] The percent of infected cells, and the number of cells are the two parameters extracted from images analysis as previously reported.[33] Data of two replicates are average.

Potency Assay of Test Compounds on M. tuberculosis (Ethionamide Concentration Fixed at 0.1 μg/mL, Serial Dilution of Test Compounds). Ethionamide (Sigma E6005-5G) is diluted into DMSO to 10 mg/mL, and aliquots are stored frozen at −20 °C. Test compounds are suspended in pure DMSO at a concentration of 40 mg/mL in Matrix tubes and then diluted by a 10-fold dilution to 4 mg/mL in Eppendorf tubes. Ten 2-fold serial dilutions of compounds are performed in DMSO in Greiner 384-well V-shape polypropylene plates (Greiner, no. 781280). Equal volumes (5 μL) of diluted

dx.doi.org/10.1021/jm500422b | J. Med. Chem. 2014, 57, 4876−4888

compounds and of ethionamide are transferred to a 384-well low volume polypropylene plate (Corning, no. 3672). Two independent replicates were done for each setting. On the day of the experiment, 0.5 μL of compound plate is first transferred by EVOBird platform (Evotec) to cell assay plates preplated with 10 μL of assay medium.

Solubility. The 10 mM solution (40 μL) in DMSO of the sample was added to 1.960 mL of MeOH or PBS at pH 7.4. The samples were gently shaken for 24 h at room temperature, then centrifuged for 5 min and filtered over 0.45 μm filters. An amount equal to 20 μL of each solution was added to 180 μL of MeOH and analyzed by LC-MS. The solubility was determined by the ratio of mass signal areas PBS/MeOH. These experiments were analyzed using a LC-MS-MS triple-quadrupole system (Varian 1200ws) under SIM or MRM detection with optimized mass parameters (declustering potential; collision energy and drying gas temperature).

Crystal Structure Determination of EthR Ligand Complexes. EthR crystals were produced by the vapor diffusion method as described previously.[35] Crystallization drops were streak seeded. The crystallization buffer contained: 1.4−1.65 M ammonium sulfate (using 0.05 M increment), 15% glycerol, and 0.1 M MES pH 6.7. The EthR ligand complexes were prepared by mixing 1 μL of ligand (33 mM in 100% DMSO) and 9 μL of the purified protein (9 mg/mL) and equilibrated for 30 min at room temperature prior crystallization. Crystals appeared within 2 days incubation at 20 °C. Crystals were flash frozen in liquid nitrogen, using mother liquor supplemented with 15% glycerol as cryoprotectant. The X-ray diffraction data were collected on a Mar CCD mosaic300 detector using synchrotron radiation on PXIII beamline (SLS, PSI, Switzerland). EthR crystals belonged to the space group $P4_12_12$, with one monomer in the asymmetric unit. Data collection statistics are summarized in Supporting Information. Indexing was performed using XDS,[36] and scaling and merging were performed using the CCP4 package.[37] Both structures were refined with the macromolecular refinement program REFMAC5. Initially ligands were fitted into the density using findligand (CCP4) and then manually positioned using Coot.[38] Six structures were deposited in the Protein Data Bank (PDB) under the accession codes.

Chemistry. *General Information.* NMR spectra were recorded on a Bruker DRX-300 spectrometer. Chemical shifts are in parts per million (ppm). The assignments were made using one-dimensional (1D) ^{1}H and ^{13}C spectra and two-dimensional (2D) HSQC and COSY spectra. Mass spectra were recorded with a LC-MS (Waters Alliance Micromass ZQ 2000). LC-MS analysis was performed using a C18 TSK-GEL Super ODS 2 μm particle size column, dimensions 50 mm × 4.6 mm. A gradient starting from 100% H_2O/0.1% formic acid and reaching 20% H_2O/80% CH_3CN/0.08% formic acid within 10 min at a flow rate of 1 mL/min was used. High-resolution mass spectra were recorded on a HPLC-MS-TOF (Waters LCT Premier). Preparative HPLC were performed using a Varian PRoStar system using an OmniSphere 10 Column C_{18} 250 mm × 41.4 mm Dynamax from Varian, Inc. A gradient starting from 20% CH_3CN/80% H_2O/0.1% formic acid and reaching 100% CH_3CN/0.1% formic acid at a flow rate of 80 mL/min or 20% MeOH/80% H_2O/0.1% formic acid reaching 100% MeOH/0.1% formic acid was used. Purity (%) was determined by reversed phase HPLC, using UV detection (215 nm), and all compounds showed purity greater than 95%. All commercial reagents and solvents were used without further purification.

*4-Iodo-N-(prop-2-ynyl)benzenesulfonamide (**3**).* To a stirred solution of propargylamine (318 μL, 4.96 mmol) and DIEA (2.30 mL, 13.2 mmol) in DCM (30 mL) was added 4-iodobenzene-1-sulfonyl chloride (1.00 g, 3.31 mmol). The mixture was stirred at room temperature for 1 h. DCM was then evaporated in vacuo. The solid was dissolved in AcOEt and washed with water and brine. The organic layer was then dried over magnesium sulfate and concentrated in vacuo. Purification of the beige solid by preparative HPLC gave the sulfonamide **3** (854 mg, 80%) as a white solid. ^{1}H NMR (300 MHz, CD_2Cl_2, 25 °C): δ = 7.95−7.92 (d, ^3J(H,H) = 8.6 Hz, 2H), 7.63−7.60 (d, ^3J(H,H) = 8.6 Hz, 2H), 4.88 (br s, 1H), 3.89−3.86 (dd, ^3J(H,H) = 6.1 Hz ^4J(H,H) = 2.5 Hz, 2H), 2.21−2.19 (t, ^4J(H,H) = 2.5 Hz, 1H). ^{13}C NMR (75 MHz, CD_2Cl_2, 25 °C): δ = 139.5, 138.4, 128.7, 100.2, 77.8, 72.9, 32.9. MS $[M - H]^-$ m/z 320. HRMS (m/z) for $C_9H_8INO_2S$ $[M - H]^-$ calculated, 319.92477; found, 319.92521.

*4-Iodo-N-isopentylbenzenesulfonamide (**4**).* To a stirred solution of 3-methylbutan-1-amine (267 μL, 2.30 mmol) in DMF (14 mL) was added 4-iodobenzenesulfonyl chloride (696 mg, 2.30 mmol) and *N*-methylmorpholine (759 μL, 6.9 mmol). The mixture was stirred at room temperature for 5 h. Water was added to the reaction mixture and the aqueous phase extracted 4 times with ethyl acetate. The combined extracts were washed with brine, dried over magnesium sulfate, and concentrated in vacuo to give the sulfonamide **4** (502 mg, 62%) as a yellow solid. ^{1}H NMR (300 MHz, CD_2Cl_2, 25 °C): δ = 7.92 (d, ^3J(H,H) = 4.7 Hz, 2H), 7.59 (d, ^3J(H,H) = 4.7 Hz, 2H), 4.71 (t, ^3J(H,H) = 5.9 Hz, 1H), 2.96 (q, ^3J(H,H) = 6.2 Hz, ^3J(H,H) = 14.7 Hz, 2H), 1.58 (n, ^3J(H,H) = 6.7 Hz, 1H), 1.34 (m, 2H), 0.84 (d, ^3J(H,H) = 6.6 Hz, 6H). MS $[M + H]^+$ m/z 354. HRMS (m/z) for $C_{11}H_{16}INO_2S$ $[M - H]^-$ calculated, 351.98737; found, 351.98865.

*General Procedure (i) for Compounds **5**, **6**, **7**, **9**, **13**, and **14**.* To a stirred solution of 3-methylbutan-1-amine (69.7 μL, 0.60 mmol) in anhydrous DMF (4.6 mL) was added 4-methylmorpholine (197.9 μL, 1.80 mmol) and the corresponding sulfonyl chloride (0.60 mmol). The mixture was stirred at room temperature until the starting material was no longer detectable by TLC, then 1 M acetic acid was then added. The precipitate was filtered, washed with water, and dried.

*N-Isopentyl-4′-methoxybiphenyl-4-sulfonamide (**5**).* Yield 143 mg of white powder, 71%. ^{1}H NMR (300 MHz, CD_2Cl_2, 25 °C): δ = 7.89 (d, ^3J(H,H) = 9.1 Hz, 2H), 7.74 (d, ^3J(H,H) = 8.5 Hz, 2H), 7.62 (d, ^3J(H,H) = 8.5 Hz, 2H), 7.04 (d, ^3J(H,H) = 9.2 Hz, 2H), 4.41 (br s, 1H), 3.88 (s, 3H), 3.00 (t, ^3J(H,H) = 7.3 Hz, 2H), 1.62 (n, ^3J(H,H) = 6.7 Hz, 1H), 1.38 (q, ^3J(H,H) = 7.4 Hz, 2H), 0.87 (d, ^3J(H,H) = 6.6 Hz, 6H). MS $[M + H]^+$ m/z 334.

*4′-Fluoro-N-isopentylbiphenyl-4-sulfonamide (**6**).* Yield 71 mg of a yellowish powder, 37%. ^{1}H NMR (300 MHz, CD_2Cl_2, 25 °C): δ = 7.92 (d, ^3J(H,H) = 8.3 Hz, 2H), 7.74 (d, ^3J(H,H) = 8.8 Hz, 2H), 7.65 (Dd, $^3J_1$(H,H) = 8.9 Hz, $^4J_2$(H,F) = 5.3 Hz, 2H), 7.22 (t, ^3J(H,F and H) = 8.8 Hz, 2H), 4.43 (br s, 1H), 3.01 (t, ^3J(H,H) = 7.2 Hz, 2H), 1.61 (n, ^3J(H,H) = 6.7 Hz, 1H), 1.38 (q, ^3J(H,H) = 7.1 Hz, 2H), 0.87 (d, ^3J(H,H) = 6.2 Hz, 6H). MS $[M + H]^+$ m/z 322.

*N-Isopentyl-4-(oxazol-5-yl)benzenesulfonamide (**7**).* Yield 78 mg of a white powder, 44%. ^{1}H NMR (300 MHz, CD_2Cl_2, 25 °C): δ = 8.02 (s, 1H), 7.93 (d, ^3J(H,H) = 8.6 Hz, 2H), 7.84 (d, ^3J(H,H) = 8.6 Hz, 2H), 7.54 (s, 1H), 4.50 (br s, 1H), 3.00 (t, ^3J(H,H) = 7.3 Hz, 2H), 1.59 (n, ^3J(H,H) = 6.7 Hz, 1H), 1.37 (q, ^3J(H,H) = 7.2 Hz, 2H), 0.86 (d, ^3J(H,H) = 6.6 Hz, 6H). MS $[M + H]^+$ m/z 295.

*N-Isopentyl-4-(1H-pyrazol-1-yl)benzenesulfonamide (**9**).* Yield 90 mg of white powder, 51%. ^{1}H NMR (300 MHz, CD_2Cl_2, 25 °C): δ = 8.09 (dd, ^3J(H,H) = 2.6 Hz, ^4J(H,H) = 0.4 Hz, 1H), 7.96 (d, ^3J(H,H) = 9.0 Hz, 2H), 7.91 (d, ^3J(H,H) = 9.2 Hz, 2H), 7.78 (d, ^3J(H,H) = 1.5 Hz, 1H), 6.57 (dd, ^3J(H,H) = 2.6 Hz, ^3J(H,H) = 1.8 Hz, 1H), 4.54 (br s, 1H), 3.00 (t, ^3J(H,H) = 7.3 Hz, 2H), 1.60 (n, ^3J(H,H) = 6.7 Hz, 1H), 1.37 (q, ^3J(H,H) = 7.2 Hz, 2H), 0.86 (d, ^3J(H,H) = 6.6 Hz, 6H). MS $[M + H]^+$ m/z 294.

*Ethyl 4-(N-Isopentylsulfamoyl)benzoate (**13**).* Yield 109 mg of white powder, 60%. ^{1}H NMR (300 MHz, CD_2Cl_2, 25 °C): δ = 8.20 (d, ^3J(H,H) = 8.7 Hz, 2H), 7.94 (d, ^3J(H,H) = 8.5 Hz, 2H), 4.46 (br s, 1H), 4.42 (q, ^3J(H,H) = 7.1 Hz, 2H), 2.99 (m, 2H), 1.59 (n, ^3J(H,H) = 6.7 Hz, 1H), 1.40 (m, 5H), 0.86 (d, ^3J(H,H) = 6.6 Hz, 6H). MS $[M + H]^+$ m/z 300.

*N-Isopentyl-4-(2-oxopyrrolidin-1-yl)benzenesulfonamide (**14**).* Yield 83 mg of white powder, 45%. ^{1}H NMR (300 MHz, CD_2Cl_2, 25 °C): δ = 7.85−7.84 (m, 4H), 4.39 (br s, 1H), 3.90 (t, ^3J(H,H) = 7.0 Hz, 2H), 2.95 (q, ^3J(H,H) = 6.7 Hz, 2H), 2.63 (t, ^3J(H,H) = 7.7 Hz, 2H), 2.20 (quint, ^3J(H,H) = 7.6 Hz, 2H), 1.55 (n, ^3J(H,H) = 6.3 Hz, 1H), 1.35 (q, ^3J(H,H) = 7.2 Hz, 2H), 0.86 (d, ^3J(H,H) = 6.7 Hz, 6H). MS $[M + H]^+$ m/z 311.

*General Procedure (ii) for Compounds **8**, **11**, and **12**.* To a stirred solution of 3-methylbutan-1-amine (69.7 μL, 0.60 mmol) in anhydrous DMF (4.6 mL) was added 4-methylmorpholine (197.9 μL, 1.80 mmol) and the corresponding sulfonyl chloride (0.60 mmol). The mixture was stirred at room temperature until the starting material was no longer detectable by TLC, then 1 M acetic acid and brine were

subsequently added. The compound was extracted with AcOEt. Organic layers were combined, dried over magnesium sulfate, and concentrated in vacuo.

*N-Isopentyl-4-(2-methylthiazol-4-yl)benzenesulfonamide (**8**).* Yield 67 mg of a pale-yellow powder, 34%. ^{1}H NMR (300 MHz, CD_2Cl_2, 25 °C): δ = 8.07 (d, ^3J(H,H) = 8.5 Hz, 2H), 7.9 (d, ^3J(H,H) = 8.5 Hz, 2H), 7.56 (s, 1H), 4.48 (t, ^3J(H,H) = 5.7 Hz,1H), 2.98 (m, 2H), 2.8 (s, 3H), 1.59 (n, ^3J(H,H) = 6.7 Hz, 1H), 1.37 (q, ^3J(H,H) = 7.2 Hz, 2H), 0.86 (d, ^3J(H,H) = 6.8 Hz,, 6H). MS $[M + H]^+$ m/z 325. HRMS (m/z) for $C_{15}H_{20}N_2O_2S_2$ $[M + H]^+$ calculated, 325.1039; found, 325.10369.

*4-Butoxy-N-isopentylbenzenesulfonamide (**11**).* Yield 55 mg of a pale-yellow powder, 30%. ^{1}H NMR (300 MHz, CD_2Cl_2, 25 °C): δ = 7.77 (d, ^3J(H,H) = 7.8 Hz, 2H), 7.01 (d, ^3J(H,H) = 9.4 Hz, 2H), 4.06 (t, ^3J(H,H) = 8.8 Hz, 2H), 2.93 (t, ^3J(H,H) = 8.1 Hz, 2H), 1.81 (q, ^3J(H,H) = 6.3 Hz, 2H), 1.55 (m, 3H), 1.01 (t, ^3J(H,H) = 7.9 Hz, 3H), 0.85 (d, ^3J(H,H) = 6.3 Hz, 6H). MS $[M + H]^+$ m/z 300.

*N,4-Diisopentylbenzenesulfonamide (**12**).* Yield 122 mg of a pale-yellow powder, 62%. ^{1}H NMR (300 MHz, CD_2Cl_2, 25 °C): δ = 7.75 (d, ^3J(H,H) = 8.5 Hz, 2H), 7.37 (d, ^3J(H,H) = 8.1 Hz, 2H), 2.95 (t, ^3J(H,H) = 7.4 Hz, 2H), 2.72 (t, ^3J(H,H) = 7.9 Hz, 2H), 1.66−1.51 (m, 4H), 1.37−1.30 (m, 2H), 0.97 (d, ^3J(H,H) = 6.3 Hz, 6H), 0.84 (d, ^3J(H,H) = 6.6 Hz, 6H). MS $[M + H]^+$ m/z 298.

*N-(4′-(N-Isopentylsulfamoyl)biphenyl-4-yl)acetamide (**10**).* A solution of Na_2CO_3 (69 mg, 0.60 mmol) in water (0.9 mL) was added to a solution of 4-iodo-*N*-isopentylbenzenesulfonamide (**4**) (141 mg, 0.40 mmol), 4-acetamidophenylboronic acid (109 mg, 0.60 mmol), and $PdCl_2$dppf (38 mg, 0.040 mmol) in DME (2.3 mL). The flask was sealed and stirred under microwave irradiation at 115 °C for 30 min. The mixture was filtered on Celite and concentrated in vacuo. Purification of the residue by preparative HPLC gave compound **10** (108 mg, 75%) as a yellowish solid. ^{1}H NMR (300 MHz, CD_2Cl_2, 25 °C): δ = 7.90 (d, ^3J(H,H) = 8.5 Hz, 2H), 7.81 (d, ^3J(H,H) = 8.5 Hz, 2H), 7.70 (d, ^3J(H,H) = 9.1 Hz, 2H), 7.66 (d, ^3J(H,H) = 8.8 Hz, 2H), 2.90 (t, ^3J(H,H) = 7.3 Hz, 2H), 2.16 (s, 3H), 1.63 (n, ^3J(H,H) = 6.7 Hz, 1H), 1.35 (q, ^3J(H,H) = 7.2 Hz, 2H), 0.85 (d, ^3J(H,H) = 6.6 Hz, 6H). MS $[M + H]^+$ m/z 361.

*General Procedure (iii) for the Synthesis of Compounds **15**, **16**, **17**, and **18**.* The corresponding amine was added to a solution of 4-(2-methylthiazol-4-yl)benzene-1-sulfonyl chloride (50 mg, 0.18 mmol) and 4-methylmorpholine (99 μL, 0.90 mmol) in dry DMF (4 mL). The mixture was stirred at room temperature for 2 h. DMF was then evaporated in vacuo. The residue was taken up in AcOEt and washed twice with water and brine. The organic layer was dried over magnesium sulfate and concentrated in vacuo.

*N-(3,3-Dimethylbutyl)-4-(2-methylthiazol-4-yl)-benzenesulfonamide (**15**).* General procedure (iii) with 3,3-dimethylbutylamine (38.7 μL, 0.27 mmol). Yield 26.5 mg of beige powder, 44%. ^{1}H NMR (300 MHz, CD_3OD, 25 °C): δ = 8.08 (d, ^3J(H,H) = 8.7 Hz, 2H), 7.88 (d, ^3J(H,H) = 8.7 Hz, 2H), 7.84 (s, 1H), 2.89 (m, 2H), 2.77 (s, 3H), 1.38 (m, 2H), 0.85 (s, 9H). ^{13}C NMR (75 MHz, CD_3OD, 25 °C): δ = 168.7, 154.4, 140.9, 139.5, 128.6, 127.8, 116.9, 44.3, 40.8, 30.5, 29.7, 18.9. MS $[M + H]^+$ m/z 339.

*4-(2-Methylthiazol-4-yl)-N-(2,2,2-trifluoroethyl)-benzenesulfonamide (**16**).* General procedure (iii) with 2,2,2-trifluoroethylamine hydrochloride (24.4 mg, 0.18 mmol). Yield 19.8 mg of a beige powder, 31%. ^{1}H NMR (300 MHz, CD_3OD, 25 °C): δ = 8.09 (d, ^3J(H,H) = 8.8 Hz, 2H), 7.91 (d, ^3J(H,H) = 8.8 Hz, 2H), 7.85 (s, 1H), 3.68 (q, ^3J(H,F) = 9.0 Hz, 2H), 2.80 (s, 3H). ^{13}C NMR (75 MHz, CD_3OD, 25 °C): δ = 168.7, 154.3, 141.2, 139.8, 125.6 (q, ^1J(C,F) = 277 Hz),117.1, 45.1 (q, $^2J^2J$(C,F) = 35 Hz), 12.9. MS $[M + H]^+$ m/z 337.

*4-(2-Methylthiazol-4-yl)-N-(3,3,3-trifluoropropyl)-benzenesulfonamide (**17**).* General procedure (iii) with 3,3,3-trifluoropropylamine hydrochloride (26.9 mg, 0.18 mmol). Yield 26.6 mg of a beige powder, 39%. ^{1}H NMR (300 MHz, CD_3OD, 25 °C): δ = 8.10 (d, ^3J(H,H) = 8.8 Hz, 2H), 7.90 (d, ^3J(H,H) = 8.8 Hz, 2H), 7.86 (s, 1H), 3.12 (t, ^3J(H,H) = 7.3 Hz, 2H), 2.77 (s, 3H), 2.39 (qt, ^3J(H,F) = 10.8 Hz, ^3J(H,H) = 7.3 Hz, 2H). ^{13}C NMR (75 MHz, CD_3OD, 25 °C): δ = 168.7, 154.3, 140.5, 139.8, 128.6, 127.9, 127.6 (q, ^1J(C,F) = 276 Hz), 117.1, 37.4 (d, ^3J(C,F) = 3.1 Hz), 35.2 (q, ^2J(C,F) = 28 Hz), 18.9; MS $[M + H]^+$ m/z 351. HRMS (m/z) for $C_{13}H_{13}F_3N_2O_2S_2$ $[M - H]^-$ calculated, 349.02978; found, 349.03032.

*4-(2-Methylthiazol-4-yl)-N-(4,4,4-trifluorobutyl)-benzenesulfonamide (**18**).* General procedure (iii) with 4,4,4-trifluorobutylamine (55.7 mg, 0.44 mmol), 100 mg (0.37 mmol) of sulfonyl chloride, 5 mL of dry DMF, and 198 μL (1.8 mmol) of 4-methylmorpholine. Yield 75 mg of beige powder, 54%. ^{1}H NMR (300 MHz, CD_3OD, 25 °C): δ = 8.09 (d, ^3J(H,H) = 8.6 Hz, 2H), 7.88 (d, ^3J(H,H) = 8.6 Hz, 2H), 7.84 (s, 1H), 2.89 (m, 2H), 2.77 (s, 3H), 1.38 (m, 2H), 0.85 (s, 9H). MS $[M + H]^+$ m/z 365.

*4-(2-Methylthiazol-4-yl)-N-(3,3,3-trifluoropropyl)benzamide (**19**).* To a stirred solution of 4-(2-methylthiazol-4-yl)benzoic acid (50.0 mg, 0.23 mmol), 3,3,3-trifluoropropylamine hydrochloride (37.5 mg, 0.25 mmol), HBTU (103 mg, 0.27 mmol), and HOBt (52 mg, 0.34 mmol) in anhydrous DMF (2.5 mL) was added DIEA (118 μL, 0.68 mmol). The mixture was stirred at room temperature for 2 h. DMF was then evaporated in vacuo. The solid was dissolved in EtOAc and washed successively with saturated K_2CO_3, HCl 1N, water, and brine. The organic layer was dried over magnesium sulfate and concentrated in vacuo to give the amide **19** (66.8 mg, 93%) as a white solid. ^{1}H NMR (300 MHz, CD_3OD, 25 °C): δ = 7.99 (d, ^3J(H,H) = 8.5 Hz, 2H), 7.87 (d, ^3J(H,H) = 8.5 Hz, 2H), 7.76 (s, 1H), 3.64 (t, ^3J(H,H) = 7.0 Hz, 2H), 2.76 (s, 3H), 2.54 (qt, ^3J(H,F) = 10.6 Hz ^3J(H,H) = 6.8 Hz, 2H). ^{13}C NMR (75 MHz, CD_3OD, 25 °C): δ = 168.4, 167.1, 153.6, 137.4, 133.1, 127.4, 126.7 (q, ^1J(C,F) = 278 Hz),125.9, 114.7, 32.7 (q, ^2J(C,F) = 28 Hz), 33.1,17.5. MS $[M + H]^+$ m/z 315. HRMS (m/z) for $C_{14}H_{13}F_3N_2OS$ $[M + H]^+$ calculated, 315.07734; found, 315.07662.

*4-(2-(Propylsulfonamidomethyl)thiazol-4-yl)-N-(3,3,3-trifluoropropyl)benzamide (**20**).* To a stirred solution of 4-acetylbenzoic acid (2.00 g, 12.2 mmol), 3,3,3-trifluoropropylamine hydrochloride (1.82 g, 12.2 mmol), HBTU (5.08 g, 13.4 mmol), and HOBt (165 mg, 1.22 mmol) in anhydrous DMF (50 mL) was added DIEA (8.44 mL, 48.8 mmol). The mixture was stirred at room temperature for 2 h. DMF is then evaporated in vacuo. The orange oil was dissolved in EtOAc and washed successively with saturated K_2CO_3 (2×), HCl 1N (2×), and brine (2×). The organic layer was dried over magnesium sulfate and concentrated in vacuo. Purification by flash column chromatography (7:3−6:4 cyclohexane−ethyl acetate) gave 4-acetyl-*N*-(3,3,3-trifluoropropyl)benzamide (**20a**) (2.98 g, 94%) as a white solid. ^{1}H NMR (300 MHz, CD_2Cl_2, 25 °C): δ = 8.02−8.00 (d, ^3J(H,H) = 8.6 Hz, 2H), 7.87−7.84 (d, ^3J(H,H) = 8.6 Hz, 2H), 6.69 (br s, 1H), 3.76−3.70 (q, ^3J(H,H) = 6.4 Hz, 2H), 2.63 (s, 3H), 2.60−2.45 (qt, ^3J(H,F) = 10.9 Hz, ^3J(H,H) = 6.6 Hz, 2H). MS $[M + H]^+$ m/z 260.

To a stirred solution of **20a** (300 mg, 1.16 mmol) in DCE (15 mL) and MeOH (6 mL) was added trimethylphenylammonium tribromide (436.1 mg, 1.16 mmol). The mixture was stirred for 1 h at 50 °C. Then 88 mg of trimethylphneylammonium tribromide was added, and the mixture was further stirred for 2 h at 50 °C. DCE and MeOH were evaporated in vacuo, and the solid was dissolved in EtOAc and washed with water and brine. The organic layer was then dried over magnesium sulfate and concentrated in vacuo to give the desired 4-(2-bromoacetyl)-*N*-(3,3,3-trifluoropropyl)benzamide **20b** (387 mg, 99%) as a white solid. MS $[M + H]^+$ m/z 340.

To a stirred solution of **20b** (500 mg, 1.48 mmol) in THF on molecular sieve (10 mL) was added *N*-benzyloxycarbonylglycine thioamide (332 mg, 1.48 mmol). The mixture was stirred for 3 h at 70 °C. THF was then evaporated in vacuo. The solid was then treated with a solution of HBr at 25% in acetic acid (5 mL) for 1 h at room temperature. Diethyl ether (40 mL) was added, and the solution was cooled to 0 °C. The precipitate was filtered, washed with diethyl ether, and dried to give a light-brown solid, which was used without any further purification. Then 75 mg of this solid was added in a 10 mL round-bottom flask, dissolved in 1.5 mL of DCM, and treated with 4-methylmorpholine (82 μL) and propane-1-sulfonyl chloride (20 μL, 0.18 mmol). The mixture was stirred at room temperature for 2 h. Then 20 μL of a new batch of propane-1-sulfonyl chloride was added, and the mixture was stirred for one additional hour. DCM was evaporated in vacuo. Purification of the residue by preparative HPLC

dx.doi.org/10.1021/jm500422b | J. Med. Chem. 2014, 57, 4876−4888

gave the final compound **20** (54 mg, 76%) as a white solid. ^{1}H NMR (300 MHz, MeOD, 25 °C): δ = 8.05−8.02 (d, ^3J(H,H) = 8.7 Hz, 2H), 7.95 (s, 1H), 7.89−7.86 (d, ^3J(H,H) = 8.7 Hz, 2H), 4.62 (s, 2H), 3.66−3.62 (t, ^3J(H,H) = 7.0 Hz, 2H), 3.13−3.08 (m, 2H), 2.62−2.46 (qt, ^3J(H,F) = 11.0 Hz ^3J(H,H) = 7.0 Hz, 2H), 1.89−1.76 (sextuplet, ^3J(H,H) = 7.6 Hz, 2H), 1.05−1.00 (t, ^3J(H,H) = 7.5 Hz, 2H). ^{13}C NMR (75 MHz, MeOD, 25 °C): δ = 170.0, 168.4, 154.1, 137.3, 133.2, 127.4, 126.6 (q, ^1J(C,F) = 275.9 Hz), 125.9, 115.4, 54.2, 43.7, 33.1 (q, ^3J(C,F) = 3.7 Hz), 32.7 (q, ^2J(C,F) = 28.1 Hz), 17.0, 11.8. MS [M − H]$^-$ m/z 434. HRMS (m/z) for $C_{17}H_{19}O_3N_3F_3S_2$ [M − H]$^-$ calculated, 434.08434; found, 409.0826.

*4-(3-(Phenylsulfonamido)prop-1-ynyl)-N-(3,3,3-trifluoropropyl)-benzamide (**21**).* In a 25 mL round-bottom flask were subsequently added DCM (8 mL), benzenesulfonyl chloride (200 μL, 1.57 mmol), DIEA (1.08 mL, 6.24 mmol), and propargylamine (129 μL, 1.88 mmol). The mixture was stirred at room temperature for 2 h. DCM was evaporated in vacuo. The residue was dissolved in AcOEt and washed twice with water and once with brine. The organic layer was then dried over magnesium sulfate and concentrated in vacuo. Purification by preparative HPLC gave *N*-(prop-2-ynyl)-benzenesulfonamide **21a** (238 mg, 78%) as a beige powder.

To a stirred solution of 4-iodobenzoic acid (300 mg, 1.21 mmol), HOBt (33 mg, 0.24 mmol), HBTU (551 mg, 1.45 mmol), and DIEA (840 μL, 4.84 mmol) in DMF over a molecular sieve (10 mL) was added 3,3,3-trifluoropropylamine hydrochloride (181 mg, 1.21 mmol). The mixture was stirred for 2 h at room temperature. DMF was then evaporated in vacuo. The residue was dissolved in AcOEt and washed with HCl 1N, saturated $NaHCO_3$, and brine. The organic layer was then dried over magnesium sulfate and concentrated in vacuo. Purification by flash column chromatography (8:2 cyclohexane-ethyl acetate) gave 4-iodo-*N*-(3,3,3-trifluoropropyl)benzamide **21b** (318 mg, 77%) as a white powder. ^{1}H NMR (300 MHz, $CDCl_3$, 25 °C): δ = 7.80 (d, ^3J(H,H) = 8.5 Hz, 2H), 7.47 (d, ^3J(H,H) = 8.5 Hz, 2H), 6.34 (br s, 1H), 3.72 (q, ^3J(H,H) = 6.3 Hz, 2H), 2.47 (qt, ^3J(H,F) = 10.7 Hz ^3J(H,H) = 6.4 Hz, 2H). LCMS (m/z) 342 [M − H]$^-$.

In a Schlenk flask were subsequently added **21b** (600 mg, 1.75 mmol), **21a** (341 mg, 1.75 mmol), $PdCl_2(PPh_3)_2$ (61.4 mg, 0.087 mmol), CuI (300 mg, 1.58 mmol), dry DMF (7.5 mL), and TEA (874 μL, 5.05 mmol) under argon. The mixture was stirred at 80 °C overnight, then cooled to room temperature and a AcOEt 1/1 NH_4Cl_{satd} mixture (15 mL) was added and stirred at room temperature for 15 min. The organic layer was washed three times with NH_4Cl_{satd}, then with water and brine. The organic layer was then dried over magnesium sulfate and concentrated in vacuo. Purification by flash column chromatography (5:95−10:90 EtOAc−DCM) gave compound **21** (311 mg, 43%) as a white powder. ^{1}H NMR (300 MHz, CD_3OD, 25 °C): δ = 7.94−7.91 (m, 2H), 7.69 (d, ^3J(H,H) = 8.4 Hz, 2H), 7.57−7.49 (m, 2H), 7.20 (d, ^3J(H,H) = 8.4 Hz, 2H), 4.06 (s, 2H), 3.61 (t, ^3J(H,H) = 7.0 Hz, 2H), 2.51 (qt, ^3J(H,F) = 10.9 Hz ^3J(H,H) = 7.0 Hz, 2H). ^{13}C NMR (75 MHz, CD_3OD, 25 °C): δ = 169.4, 142.3, 134.9, 133.7, 132.6, 130.1, 128.4, 128.1, 127.2, 87.7, 84.0, 34.5 (q, ^3J(C,F) = 3.9 Hz), 34.0 (q, ^2J(C,F) = 28.2 Hz), 33.9. MS [M + H]$^+$ m/z 411. HRMS (m/z) for $C_{19}H_{17}F_3N_2O_3S$ [M − H]$^-$ calculated, 409.08413; found, 409.08404.

■ ASSOCIATED CONTENT

Ⓢ Supporting Information

List of arylsulfonyl chlorides and amines used for in silico chemical library synthesis and data collection statistics. This material is available free of charge via the Internet at http://pubs.acs.org.

Accession Codes

The following codes have been deposited in the Protein Data Bank: **20**, 4M3E; **21**, 4M3D; **8**, 4M3F; **17**, 4M3G; **19**, 4M3B.

■ AUTHOR INFORMATION

Corresponding Authors

*For N.W.: phone, +33 (0)320 964 991; fax, +33 (0) 320 964 709; e-mail, nicolas.willand@univ-lille2.fr. Websites: U761, http://www.deprezlab.fr; PRIM, http://www.drugdiscoverylille.org.

*For B.D.: phone, +33 (0)320 964 924; fax, +33 (0) 320 964 709; e-mail: benoit.deprez@univ-lille2.fr.

Present Address

△Center of Excellence, Helwan Structure Biology Research, Faculty of Pharmacy, Helwan University, Cairo, Egypt.

Notes

The authors declare no competing financial interest.

■ ACKNOWLEDGMENTS

We thank Dr. Zoé Lens for technical assistance. We are grateful to the institutions that support our laboratory (Inserm), INSERM-Avenir fellowship to Priscille Brodin, Institut Pasteur Korea (grants: K204EA000001-08E0100-00100 and K204EA000001-09E0100-00100), Universite Lille Nord de France, Institut Pasteur de Lille, CNRS, EU, Région Nord-Pas de Calais, FEDER (no. 09220019 and 09220020 PRESAGE 31510), ANR (ANR-06-EMPB-033), and PRIM, Pôle de Recherche Interdisciplinaire du Médicament. René Wintjens is Research Associate at the Belgian Fund for Scientific Research (FNRS). Data management was performed using Pipeline Pilot from Accelrys. We thank VARIAN Inc. for their technical support. RMN acquisitions were done at the LARMN, Lille.

■ ABBREVIATIONS USED

AcOEt, ethyl acetate; CH_3CN, acetonitrile; DCE, 1,2-dichloroethane; DCM, dichloromethane; DIEA, diisopropylethylamine; DME, dimethoxyethane; DMF, dimethylformamide; DMSO, dimethyl sulfoxide; DTT, dithiothreitol; ETH, ethionamide; FBDD, fragment-based drug design; HAC, heavy atom count; HBTU, *O*-benzotriazole-*N*,*N*,*N*′,*N*′-tetramethyluronium hexafluorophosphate; HOBt, *N*-hydroxybenzotriazole; HTS, high throughput screening; MDR-TB, multidrug resistant tuberculosis; MeOH, methanol; MIC, minimal inhibitory concentration; NMP, 4-methylmorpholine; PBS, phosphate buffered saline; RMSD, root-mean-square deviation; SAR, structure−activity relationships; SPR, surface plasmon resonance; TB, tuberculosis; TEA, triethylamine; THF, tetrahydrofuran; TLC, thin layer chromatography; T_m, melting temperature; TSA, thermal shift assay

■ REFERENCES

(1) *Global Tuberculosis Control*; World Health Organization: Geneva, 2013.

(2) Koul, A.; Arnoult, E.; Lounis, N.; Guillemont, J.; Andries, K. The challenge of new drug discovery for tuberculosis. *Nature* **2011**, *469*, 483−490.

(3) Villemagne, B.; Crauste, C.; Flipo, M.; Baulard, A. R.; Déprez, B.; Willand, N. Tuberculosis: the drug development pipeline at a glance. *Eur. J. Med. Chem.* **2012**, *51*, 1−16.

(4) Zumla, A.; Nahid, P.; Cole, S. T. Advances in the development of new tuberculosis drugs and treatment regimens. *Nature Rev. Drug Discovery* **2013**, *12*, 388−404.

(5) Payne, D. J.; Gwynn, M. N.; Holmes, D. J.; Pompliano, D. L. Drugs for bad bugs: confronting the challenges of antibacterial discovery. *Nature Rev. Drug Discovery* **2007**, *6*, 29−40.

(6) Cole, S. T.; Riccardi, G. New tuberculosis drugs on the horizon. *Curr. Opin. Microbiol.* **2011**, *14*, 570−576.
(7) Chessari, G.; Woodhead, A. J. From fragment to clinical candidate—a historical perspective. *Drug Discovery Today* **2009**, *14*, 668−675.
(8) Congreve, M.; Chessari, G.; Tisi, D.; Woodhead, A. J. Recent developments in fragment-based drug discovery. *J. Med. Chem.* **2008**, *51*, 3661−3680.
(9) Manger, M.; Scheck, M.; Prinz, H.; von Kries, J. P.; Langer, T.; Saxena, K.; Schwalbe, H.; Fürstner, A.; Rademann, J.; Waldmann, H. Discovery of *Mycobacterium tuberculosis* protein tyrosine phosphatase A (MptpA) inhibitors based on natural products and a fragment-based approach. *ChemBioChem* **2005**, *6*, 1749−1753.
(10) Rawls, K. A.; Therese Lang, P.; Takeuchi, J.; Imamura, S.; Baguley, T. D.; Grundner, C.; Alber, T.; Ellman, J. A. Fragment-based discovery of selective inhibitors of the *Mycobacterium tuberculosis* protein tyrosine phosphatase PtpA. *Bioorg. Med. Chem. Lett.* **2009**, *19*, 6851−6854.
(11) Soellner, M. B.; Rawls, K. A.; Grundner, C.; Alber, T.; Ellman, J. A. Fragment-based substrate activity screening method for the identification of potent inhibitors of the *Mycobacterium tuberculosis* phosphatase PtpB. *J. Am. Chem. Soc.* **2007**, *129*, 9613−9615.
(12) Alvin, W. H.; Silvestre, H. L.; Shijun, W.; Alessio, C.; Tom, L. B.; Chris, A. Application of fragment growing and fragment linking to the discovery of inhibitors of *Mycobacterium tuberculosis* pantothenate synthetase. *Angew. Chem., Int. Ed.* **2009**, *48*, 8452−8456.
(13) Scheich, C.; Puetter, V.; Schade, M. Novel small molecule inhibitors of MDR *Mycobacterium tuberculosis* by NMR fragment screening of antigen 85C. *J. Med. Chem.* **2010**, *53*, 8362−8367.
(14) Hudson, S. A.; McLean, K. J.; Surade, S.; Yang, Y.-Q.; Leys, D.; Ciulli, A.; Munro, A. W.; Abell, C. Application of fragment screening and merging to the discovery of inhibitors of the *Mycobacterium tuberculosis* cytochrome P450 CYP121. *Angew. Chem., Int. Ed.* **2012**, *51*, 9311−9316.
(15) Hudson, S. A.; Surade, S.; Coyne, A. G.; McLean, K. J.; Leys, D.; Munro, A. W.; Abell, C. Overcoming the limitations of fragment merging: rescuing a strained merged fragment series targeting *Mycobacterium tuberculosis* CYP121. *ChemMedChem* **2013**, *8*, 1451−1456.
(16) Tran, A. T.; West, N. P.; Britton, W. J.; Payne, R. J. Elucidation of *Mycobacterium tuberculosis* type II dehydroquinase inhibitors using a fragment elaboration strategy. *ChemMedChem* **2012**, *7*, 1031−1043.
(17) Surade, S.; Nancy, T.; Hengrung, N.; Lechartier, B.; Cole, S. T.; Abell, C.; Blundell, T. L. A structure-guided fragment-based approach for the discovery of allosteric inhibitors targeting the lipophilic binding site of transcription factor EthR. *Biochem. J.* **2014**, *458*, 387−394.
(18) Chambers, H. F.; Moreau, D.; Yajko, D.; Miick, C.; Wagner, C.; Hackbarth, C.; Kocagöz, S.; Rosenberg, E.; Hadley, W. K.; Nikaido, H. Can penicillins and other beta-lactam antibiotics be used to treat tuberculosis? *Antimicrob. Agents Chemother.* **1995**, *39*, 2620−2624.
(19) Vannelli, T. A.; Dykman, A.; Ortiz de Montellano, P. R. The antituberculosis drug ethionamide is activated by a flavoprotein monooxygenase. *J. Biol. Chem.* **2002**, *277*, 12824−12829.
(20) Baulard, A. R.; Betts, J. C.; Engohang-Ndong, J.; Quan, S.; McAdam, R. A.; Brennan, P. J.; Locht, C.; Besra, G. S. Activation of the pro-drug ethionamide is regulated in mycobacteria. *J. Biol. Chem.* **2000**, *275*, 28326−28331.
(21) DeBarber, A. E.; Mdluli, K.; Bosman, M.; Bekker, L. G.; Barry, C. E., III. Ethionamide activation and sensitivity in multidrug-resistant *Mycobacterium tuberculosis*. *Proc. Natl. Acad. Sci. U. S. A.* **2000**, *97*, 9677−9682.
(22) Willand, N.; Dirie, B.; Carette, X.; Bifani, P.; Singhal, A.; Desroses, M.; Leroux, F.; Willery, E.; Mathys, V.; Deprez-Poulain, R.; Delcroix, G.; Frenois, F.; Aumercier, M.; Locht, C.; Villeret, V.; Deprez, B.; Baulard, A. R. Synthetic EthR inhibitors boost antituberculous activity of ethionamide. *Nature Med.* **2009**, *15*, 537−544.
(23) Flipo, M.; Desroses, M.; Lecat-Guillet, N.; Dirié, B.; Carette, X.; Leroux, F.; Piveteau, C.; Demirkaya, F.; Lens, Z.; Rucktooa, P.; Villeret, V.; Christophe, T.; Jeon, H. K.; Locht, C.; Brodin, P.; Déprez, B.; Baulard, A. R.; Willand, N. Ethionamide boosters: synthesis, biological activity, and structure−activity relationships of a series of 1,2,4-oxadiazole EthR inhibitors. *J. Med. Chem.* **2011**, *54*, 2994−3010.
(24) Flipo, M.; Desroses, M.; Lecat-Guillet, N.; Villemagne, B.; Blondiaux, N.; Leroux, F.; Piveteau, C.; Mathys, V.; Flament, M.-P.; Siepmann, J.; Villeret, V.; Wohlkönig, A.; Wintjens, R.; Soror, S. H.; Christophe, T.; Jeon, H. K.; Locht, C.; Brodin, P.; Déprez, B.; Baulard, A. R.; Willand, N. Ethionamide boosters. 2. Combining bioisosteric replacement and structure-based drug design to solve pharmacokinetic issues in a series of potent 1,2,4-oxadiazole EthR inhibitors. *J. Med. Chem.* **2012**, *55*, 68−83.
(25) Flipo, M.; Willand, N.; Lecat-Guillet, N.; Hounsou, C.; Desroses, M.; Leroux, F.; Lens, Z.; Villeret, V.; Wohlkönig, A.; Wintjens, R.; Christophe, T.; Kyoung Jeon, H.; Locht, C.; Brodin, P.; Baulard, A. R.; Déprez, B. Discovery of novel *N*-phenylphenoxyacetamide derivatives as EthR inhibitors and ethionamide boosters by combining high-throughput screening and synthesis. *J. Med. Chem.* **2012**, *55*, 6391−6402.
(26) Willand, N.; Desroses, M.; Toto, P.; Dirié, B.; Lens, Z.; Villeret, V.; Rucktooa, P.; Locht, C.; Baulard, A.; Deprez, B. Exploring drug target flexibility using in situ click chemistry: application to a mycobacterial transcriptional regulator. *ACS Chem. Biol.* **2010**, *5*, 1007−1013.
(27) Rees, D. C.; Congreve, M.; Murray, C. W.; Carr, R. Fragment-based lead discovery. *Nature Rev. Drug Discovery* **2004**, *3*, 660−672.
(28) Jhoti, H.; Williams, G.; Rees, D. C.; Murray, C. W. The 'rule of three' for fragment-based drug discovery: where are we now? *Nature Rev. Drug Discovery* **2013**, *12*, 644−645.
(29) Hopkins, A. L.; Groom, C. R.; Alex, A. Ligand efficiency: a useful metric for lead selection. *Drug Discovery Today* **2004**, *9*, 430−431.
(30) Hopkins, A. L.; Keseru, G. M.; Leeson, P. D.; Rees, D. C.; Reynolds, C. H. The role of ligand efficiency metrics in drug discovery. *Nature Rev. Drug Discovery* **2014**, *13*, 105−121.
(31) Hagmann, W. K. The many roles for fluorine in medicinal chemistry. *J. Med. Chem.* **2008**, *51*, 4359−4369.
(32) Christophe, T.; Jackson, M.; Jeon, H. K.; Fenistein, D.; Contreras-Dominguez, M.; Kim, J.; Genovesio, A.; Carralot, J.-P.; Ewann, F.; Kim, E. H.; Lee, S. Y.; Kang, S.; Seo, M. J.; Park, E. J.; Škovierová, H.; Pham, H.; Riccardi, G.; Nam, J. Y.; Marsollier, L.; Kempf, M.; Joly-Guillou, M.-L.; Oh, T.; Shin, W. K.; No, Z.; Nehrbass, U.; Brosch, R.; Cole, S. T.; Brodin, P. High content screening identifies decaprenyl-phosphoribose 2′ epimerase as a target for intracellular antimycobacterial inhibitors. *PLoS Pathog.* **2009**, *5*, e1000645.
(33) Christophe, T.; Ewann, F.; Jeon, H. K.; Cechetto, J.; Brodin, P. High-content imaging of *Mycobacterium tuberculosis*-infected macrophages: an in vitro model for tuberculosis drug discovery. *Future Med. Chem.* **2010**, *2*, 1283−1293.
(34) Brodin, P.; Christophe, T. High-content screening in infectious diseases. *Curr. Opin. Chem. Biol.* **2011**, *15*, 534−539.
(35) Dover, L. G.; Corsino, P. E.; Daniels, I. R.; Cocklin, S. L.; Tatituri, V.; Besra, G. S.; Futterer, K. Crystal structure of the TetR/CamR family repressor *Mycobacterium tuberculosis* EthR implicated in ethionamide resistance. *J. Mol. Biol.* **2004**, *340*, 1095−1105.
(36) Kabsch, W. XDS. *Acta Crystallogr., Sect. D: Biol. Crystallogr.* **2010**, *66*, 125−132.
(37) The CCP4 suite: programs for protein crystallography. *Acta Crystallogr., Sect. D: Biol. Crystallogr.* **1994**, *50*, 760−763.
(38) Emsley, P.; Lohkamp, B.; Scott, W. G.; Cowtan, K. Features and development of Coot. *Acta Crystallogr., Sect. D: Biol. Crystallogr.* **2010**, *66*, 486−501.